




Hybrid Cathodic/Anodic Electrosynthesis of Phase Pure $\text{Ag}_4\text{V}_2\text{O}_7$ Thin Films

Abbas Vali,¹ Soo Yeon Kim,² Fahad Danladi,¹ Abhishek Rawat,¹ Chuzhong Zhang,³ Peter S. Toth,⁴ Csaba Janáky,⁴ Noseung Myung,² Efstathios I. Meletis,³ and Krishnan Rajeshwar^{1,*} 

¹Department of Chemistry & Biochemistry, The University of Texas at Arlington, Arlington, Texas 76109, United States of America

²Department of Applied Chemistry, Konkuk University Glocal Campus, Chungju, Chungbuk 27478, Republic of Korea

³Department of Materials Science and Engineering, The University of Texas at Arlington, Arlington, Texas 76019, United States of America

⁴Department of Physical Chemistry and Materials Science, University of Szeged, Szeged, H-6720, Hungary

Here, we demonstrate a two-step electrosynthesis approach for the preparation of silver pyrovanadate, $\text{Ag}_4\text{V}_2\text{O}_7$ in thin-film form. In the first, cathodic step, polycrystalline Ag was deposited on fluorine doped tin oxide (FTO) substrate from a non-aqueous bath. Aqueous pyrovanadate species were then generated by aging of a CO_2 -infused sodium orthovanadate (Na_3VO_4) solution for three weeks. Silver ions were subsequently generated in situ in this medium using anodic stripping of the Ag/FTO films from the first step. Interfacial precipitation of the Ag^+ ions with the pyrovanadate species afforded the targeted product in phase pure form. The various stages of the electrosynthesis were monitored in situ via the combined use of voltammetry, electrochemical quartz crystal nanogravimetry (EQCN), and coulometry. The $\text{Ag}_4\text{V}_2\text{O}_7$ thin films were characterized by a variety of experimental techniques, including X-ray diffraction, laser Raman spectroscopy, diffuse reflectance spectroscopy, scanning electron microscopy, and high-resolution transmission electron microscopy. Surface photovoltage spectroscopy, ambient-pressure photoemission spectroscopy, and Kelvin probe contact potential difference (work function) measurements afforded information on the energy band structure of the *p*-type $\text{Ag}_4\text{V}_2\text{O}_7$ semiconductor. Finally, the electrochemical and photoelectrochemical properties of the electrosynthesized $\text{Ag}_4\text{V}_2\text{O}_7$ thin films were studied in both aqueous and non-aqueous electrolytes.

© 2023 The Electrochemical Society ("ECS"). Published on behalf of ECS by IOP Publishing Limited. [DOI: 10.1149/1945-7111/acd149]

Manuscript submitted March 13, 2023; revised manuscript received April 22, 2023. Published May 15, 2023.

Supplementary material for this article is available [online](#)

The Ag-V-O phase space features several compounds that have evoked interest from both fundamental and practical perspectives.¹ These compounds may be described in terms of the relative mole ratios of the corresponding binary compounds in combination. Thus, a wide range of known compound stoichiometries (1:7, 1:2, 1:1, 2:1, 3:1) coupled with the occurrence of polymorphs for many of these compounds impart a richness and diversity to the underlying solid-state chemistry. The present study² focuses on the first electrosynthesis of one such compound, silver pyrovanadate, $\text{Ag}_4\text{V}_2\text{O}_7$, in which Ag_2O and V_2O_5 combine in a 2:1 mole ratio. As with silver metavanadate, AgVO_3 and silver orthovanadate, Ag_3VO_4 , $\text{Ag}_4\text{V}_2\text{O}_7$ is also a low bandgap (~ 2 eV) semiconductor, making these compounds potential candidates for solar energy conversion, including photovoltaics, water splitting, and as photocatalysts for environmental pollutant decomposition.¹

Hydrothermal synthesis has been predominantly used for preparing $\text{Ag}_4\text{V}_2\text{O}_7$; other methods for making powders of this material include solid state, hydrothermal, dynamic template, molten salt flux, and solution precipitation.^{3–16} However, solar energy conversion schemes demand the active material to be compatible with scale up and deployment in large area modules. Thin films are eminently suited to this scenario and electrochemical deposition^{17–22} delivers the target material in thin film form on conductive substrates. In this vein, a hybrid cathodic/anodic electrosynthesis scheme is described below for the preparation of $\text{Ag}_4\text{V}_2\text{O}_7$ thin films on fluorine doped tin oxide (FTO) substrate (see scheme in Fig. 1).

Experimental

Materials.—Silver nitrate, AgNO_3 (Alfa Aesar) and sodium orthovanadate, Na_3VO_4 (Alfa Aesar) were used as the Ag and V precursor source, respectively. Acetonitrile, CH_3CN (Sigma-Aldrich) and double-distilled water were used as solvents as needed.

Other chemicals were as described in Refs. 23–25; all were used as received without further purification.

Physical characterization.—Instrumentation details for X-ray diffraction (XRD), energy-dispersive X-ray analysis (EDX), diffuse reflectance spectroscopy (DRS), surface photovoltage spectroscopy (SPS) and ambient pressure UV photoelectron spectroscopy (AP-UPS) are given elsewhere.^{23–25} Scanning electron microscopy (SEM) was conducted using a Hitachi S-3000 N FE scanning electron microscope, operating at 25 kV. High-resolution transmission electron microscopy (HRTEM) was performed on a Hitachi H-9500, operating at an acceleration voltage of 300 kV. Samples for HRTEM were prepared by carefully scratching off the as-deposited $\text{Ag}_4\text{V}_2\text{O}_7$ layer from the FTO substrate and subsequently dispersing the nanoparticles in ethanol. This suspension was drop cast onto a carbon coated copper grid (Electron Microscopy Sciences). Laser Raman spectra were acquired on a Thermo Scientific DXR Raman microscope, using a laser excitation line of 633 nm (1.96 eV) with a 50 \times objective and an incident power, ≤ 3.0 mW.

Electrochemical/photoelectrochemical characterization.—Instrumentation, electrochemical cell, and illumination source details for voltammetry, photoelectrochemistry experiments and EQCN, are given elsewhere.^{23–26}

Electrosynthesis.—The silver electrodeposition step and details associated with the second anodic stripping step (Fig. 1) were given elsewhere. Briefly, potentiodynamic film growth was used in the first step and the potential was swept 10 times from +0.1 to -0.70 V at 25 mV s^{-1} scan rate and 20 s resting time between cycles. The silver thin film on FTO substrate with 0.785 cm^2 area served as a working electrode. A platinum foil and $\text{Ag}/\text{AgCl}/3 \text{ M NaCl}$ were used as the counter-electrode and reference electrode, respectively.

For the second step, sodium orthovanadate, Na_3VO_4 was used as the precursor species. 0.3237 g of Na_3VO_4 was dissolved in 40 ml of DI water in a 50 ml beaker. The pH of the fresh solution was 12.2

*Electrochemical Society Fellow.

^zE-mail: rajeshwar@uta.edu

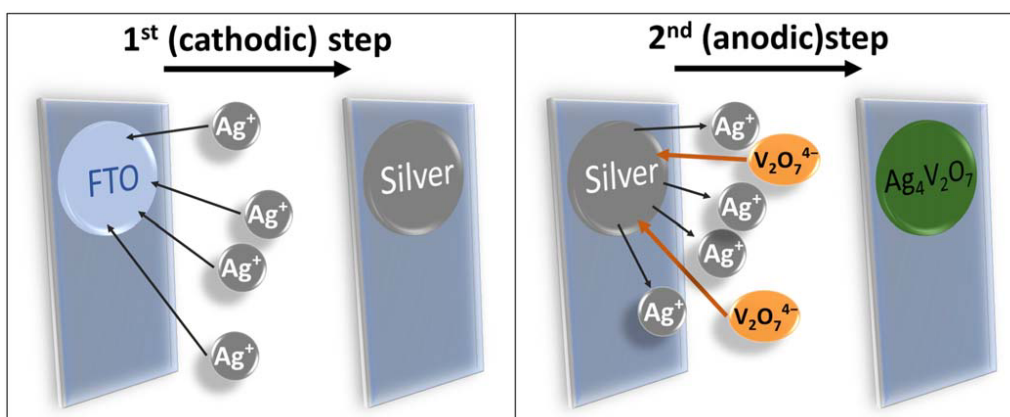
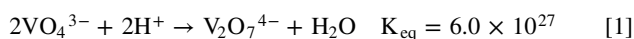


Figure 1. Two step electrochemical synthesis of $\text{Ag}_4\text{V}_2\text{O}_7$. In the first, cathodic step shown on the left, silver is electrodeposited on a FTO surface. In the second step (right frame), the silver is anodically stripped in an aqueous medium containing pyrovanadate species ($\text{V}_2\text{O}_7^{4-}$) and resulting in in situ precipitation of a $\text{Ag}_4\text{V}_2\text{O}_7$ film on the FTO surface. Refer to text for further details.

due to base hydrolysis. The beaker was sealed with Parafilm and the prepared solution was aged for three weeks to produce pyrovanadate ions ($\text{V}_2\text{O}_7^{4-}$). CO_2 was diffused through the sodium orthovanadate solution during the aging process to produce protons from carbonic acid dissociation. Thus, the solution pH decreases during the aging process (Fig. S1). However, protons are needed for the dimerization reaction (Reaction 1).



This reaction was accompanied by proton consumption and by a gradual change of the initially colorless solution to one with a yellow tinge (Fig. S2).

For the preparation of $\text{Ag}_4\text{V}_2\text{O}_7$ thin film, the potential of the silver/FTO electrode was continuously swept at 10 mV s^{-1} from +1.2 to +1.4 V. The potentiodynamic process was stopped when there was no more change in the anodic current.

Since the electrodeposition of silver was carried out by passing $\sim 0.13 \text{ C cm}^{-2}$ in each potentiodynamic cycle in the first step, the number of moles of electrodeposited silver can be coulometrically assayed using Faraday's Law. Then, the number of moles of $\text{Ag}_4\text{V}_2\text{O}_7$ could then be estimated from the formation/stripping reactions from which the mass of $\text{Ag}_4\text{V}_2\text{O}_7$ was calculated. By taking the density of $\text{Ag}_4\text{V}_2\text{O}_7$ as 5.9 g cm^{-3} ,¹² the volume of deposited $\text{Ag}_4\text{V}_2\text{O}_7$ was calculated and divided by the working electrode area to obtain the nominal film thickness as $\sim 1.4 \mu\text{m}$.

Results and Discussion

Two-step $\text{Ag}_4\text{V}_2\text{O}_7$ electrochemical synthesis.—The heart of this process is the in situ precipitation of anodically-generated Ag^+ ions with $\text{V}_2\text{O}_7^{4-}$ (Reaction 2) which is driven by the low solubility product for $\text{Ag}_4\text{V}_2\text{O}_7$ ($K_{\text{sp}} = 2.0 \times 10^{-14}$).²⁷ Importantly, a solution with pH ~ 9.4 is needed for the anodic stripping step to provide the dominant $\text{V}_2\text{O}_7^{4-}$ species required for subsequent $\text{Ag}_4\text{V}_2\text{O}_7$ film growth. For example, consultation of Pourbaix diagrams show that in the high pH (~ 12.2) range, VO_4^{3-} species and in the pH range around ~ 7.0 , VO_3^- species will be dominant.^{23,24,28}

As a result of precipitation, a brownish yellow $\text{Ag}_4\text{V}_2\text{O}_7$ film is formed on the FTO substrate (Fig. S3A).



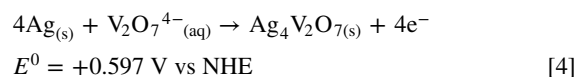
Figure 2A contains a linear sweep voltammogram (red line) and the corresponding EQCN frequency change (blue line) during anodic stripping. The frequency decrease along the oxidation wave domain is diagnostic of mass gain and the electrodeposition of a film (presumably $\text{Ag}_4\text{V}_2\text{O}_7$) on the Pt-coated quartz surface. To confirm that the frequency change is only due to formation of $\text{Ag}_4\text{V}_2\text{O}_7$, a

linear voltammetry sweep was coupled with monitoring of the corresponding EQCN frequency change during anodic polarization of a bare Pt electrode in $22 \text{ mM V}_2\text{O}_7^{4-}$ contained solution, Fig. S4. No oxidation wave or frequency change were observed during the control experiment underlining that the silver precursor film is an integral part of the target film formation.

The EQCN and coulometric data for the oxidation of silver may be combined via the Sauerbrey equation:^{29,30}

$$Q = -\left(\frac{nFk}{M}\right)\Delta f \quad [3]$$

Here, Q is the charge consumed, F is the Faraday constant, Δf is the frequency change, k is the Sauerbrey constant,^{29,30} and M is the molar mass of the deposit. By constructing a Q versus $-\Delta f$ "Sauerbrey plot" (Fig. 2B), the electron stoichiometry, n for film formation may be computed from the slope. The calculated n value from the least-squares fitted slope was 4.04, very close to the value expected from the following reaction:



The slight but unmistakable lag in the mass gain or frequency change onset relative to the current flow onset in Fig. 2A is reminiscent of the trends seen earlier for AgVO_3 and Ag_3VO_4 . This lag signals the fact that nucleation/growth of $\text{Ag}_4\text{V}_2\text{O}_7$ is also a kinetically controlled process.

Structure and morphological aspects.—Morphological examination of the as-prepared sample by SEM revealed film nucleation/growth in the form of nanorods, Fig. 3. A similar morphology has been reported for $\text{Ag}_4\text{V}_2\text{O}_7$ prepared by other methods (hydrothermal synthesis).¹⁴ Elemental EDX maps (not shown) indicated uniform film deposition across the entire FTO surface. Specifically, no regions rich in silver could be found, for example. Compositional EDX assays averaged from different spots of sample were consistent with a Ag/V ratio: 2.11 ± 0.07 ; a representative EDX trace is shown in Fig. S5.

Figures 4 and S6 contain TEM images and selected area electron diffraction (SAED) patterns for different points of as-prepared $\text{Ag}_4\text{V}_2\text{O}_7$. SAED patterns (Figs. 4B and S6C) revealed features attributable to a mixture of single crystal and polycrystalline phases.

The estimated d-spacing values from SAED data for single crystalline part (see Fig. 4B) and polycrystalline part (see Fig. S6C) in this study along with estimated d-spacing values from XRD data in Ref. 12 are represented in Tables SI and SII, respectively. These results show that the estimated interplanar spacing from SAED

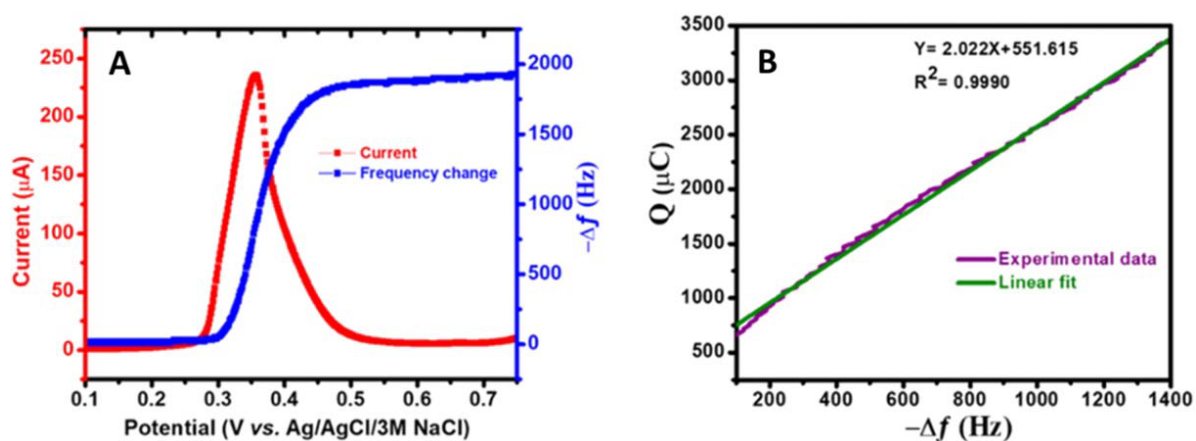


Figure 2. (A) Linear sweep voltammogram and the corresponding EQCN frequency change for the electrodeposition of silver pyrovanadate at 10 mV s^{-1} potential scan rate. (B) A Sauerbrey plot derived from the EQCN-voltammetry data (see text).

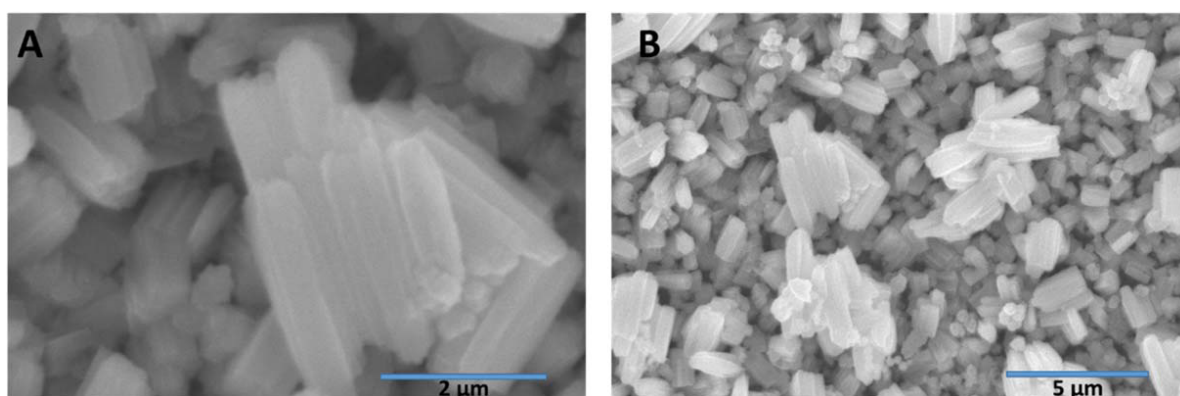


Figure 3. Representative scanning electron micrographs of an as-prepared $\text{Ag}_4\text{V}_2\text{O}_7$ film on FTO substrate at two different magnifications.

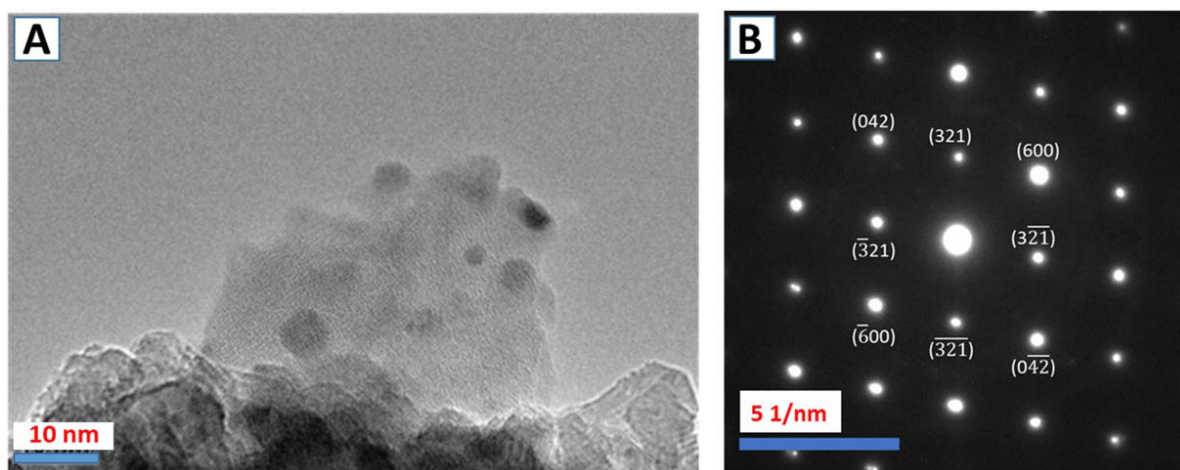


Figure 4. High resolution TEM (A) and SAED (B) images for as-prepared $\text{Ag}_4\text{V}_2\text{O}_7$. Scale bar in B corresponds to 5 nm^{-1} .

analysis are in good agreement with those calculated using XRD data for reference $\text{Ag}_4\text{V}_2\text{O}_7$.

Significantly, XRD data on the as-prepared film (Fig. 5) supported the TEM data in that the synthesized film was crystalline (*even without thermal anneal*) in phase pure $\text{Ag}_4\text{V}_2\text{O}_7$ form. In other words, the films were crystalline even though the electrodeposition was performed at room temperature. Non-optimal film morphology (amorphous nature) and contamination with side products are

perennial Achilles heels of the electrosynthesis approach. However, the present study demonstrates that these handicaps are not always problematic and good crystallinity can be obtained even under mild process conditions in favorable cases.

The as-prepared silver vanadate samples were analyzed by laser Raman spectroscopy to investigate the degree of structural order—disorder, as well as to confirm phase purity. Figure 6 shows a Raman spectrum of $\text{Ag}_4\text{V}_2\text{O}_7$ synthesized under optimal conditions. The

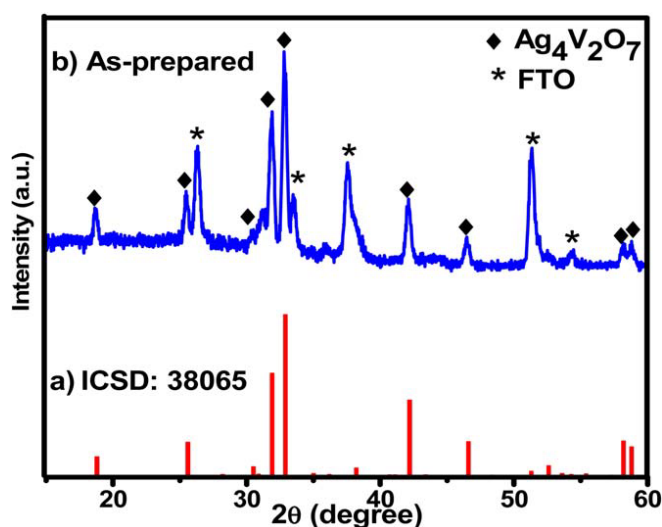


Figure 5. XRD patterns for (a) reference $\text{Ag}_4\text{V}_2\text{O}_7$ and (b) electrodeposited sample.

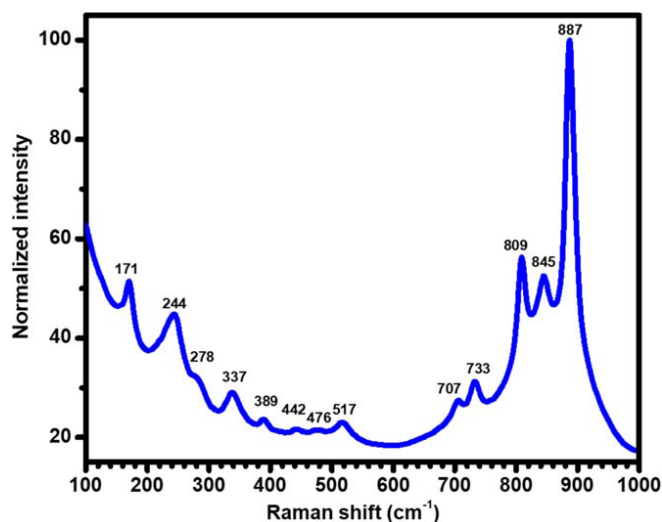


Figure 6. Laser Raman spectrum of as-prepared silver pyrovanadate sample.

spectrum of $\text{Ag}_4\text{V}_2\text{O}_7$ is characterized by a single band at about 887 cm^{-1} due to stretching vibration of O–V–O or Ag–O–Ag bridges. Two Raman-active modes at 809 and 845 cm^{-1} correspond to the stretching vibrations of Ag–O–Ag bridges and VO groups in $\text{V}_2\text{O}_7^{4-}$ ions, respectively.¹⁵ Also, the bands at 517 and 733 cm^{-1} reflect symmetric and asymmetric stretching modes of V–O–V bridges, respectively. The Raman-active mode at 707 cm^{-1} is assigned to V–O–Ag bridging. The Raman bands at 244 , 278 , and 389 cm^{-1} may be assigned to OVO_3/VO_3 bending vibration modes.²⁵ These bands along with those located at 244 and 171 cm^{-1} were in good agreement with those reported for $\text{Ag}_4\text{V}_2\text{O}_7$ prepared using chemical precipitation method.¹⁵

The as-prepared $\text{Ag}_4\text{V}_2\text{O}_7$ film was annealed at four different temperatures ($100\text{ }^\circ\text{C}$, $150\text{ }^\circ\text{C}$, $200\text{ }^\circ\text{C}$, and $225\text{ }^\circ\text{C}$) for 30 min to study the effect of anneal temperature on crystallinity and thermal stability of the as-prepared sample. The XRD results (Fig. S7) showed that the crystalline phase of the as-prepared sample after anneal at $100\text{ }^\circ\text{C}$ and $150\text{ }^\circ\text{C}$ was not changed, and the film remained in the $\text{Ag}_4\text{V}_2\text{O}_7$ form. On the other hand, the XRD pattern of the annealed sample at $200\text{ }^\circ\text{C}$ showed that the $\text{Ag}_4\text{V}_2\text{O}_7$ peaks had disappeared. Further increasing the anneal temperature to $225\text{ }^\circ\text{C}$ decomposed completely the $\text{Ag}_4\text{V}_2\text{O}_7$ film to $\text{Ag}_2\text{V}_4\text{O}_{11}$ and silver. The sample also changed color (Fig. S3B).

Optical behavior.—The UV/visible spectrum of an as-prepared sample showed an absorption onset wavelength of $\sim 530\text{ nm}$ (see Fig. S8). Table I presents a comparison of this value with those reported in the literature for $\text{Ag}_4\text{V}_2\text{O}_7$ samples prepared using other synthesis methods. There is some scatter in the reported values due to the uncertainty in the estimation of the onset value from the spectral information. Nonetheless, a safe conclusion can be made that the onset wavelength cut-off for electrodeposited $\text{Ag}_4\text{V}_2\text{O}_7$ is in the range: $496\text{--}530\text{ nm}$.

Tauc plots^{33–35} were constructed from the UV/visible DRS data. Figures 7A and 7B contain these plots for direct and indirect optical transitions in the as-deposited $\text{Ag}_4\text{V}_2\text{O}_7$ sample; the corresponding energy band gaps were $2.58 \pm 0.04\text{ eV}$ and $2.52 \pm 0.02\text{ eV}$, respectively. Table II presents a comparison of these values with those reported in the literature for samples derived from other synthetic methods. There is some scatter in the reported values of the energy band gaps (Table II). This issue has been addressed by us and other authors elsewhere.^{34,35}

Electronic band structure.—Ambient-pressure UV photoelectron spectroscopy (AP-UPS)³⁶ was used to map the valence band maximum (VBM) in $\text{Ag}_4\text{V}_2\text{O}_7$. Figure S9A contains the data; the VBM is located at the intercept of the plot. A value of VBM $-4.91 \pm 0.05\text{ eV}$ on the vacuum energy scale, was estimated.

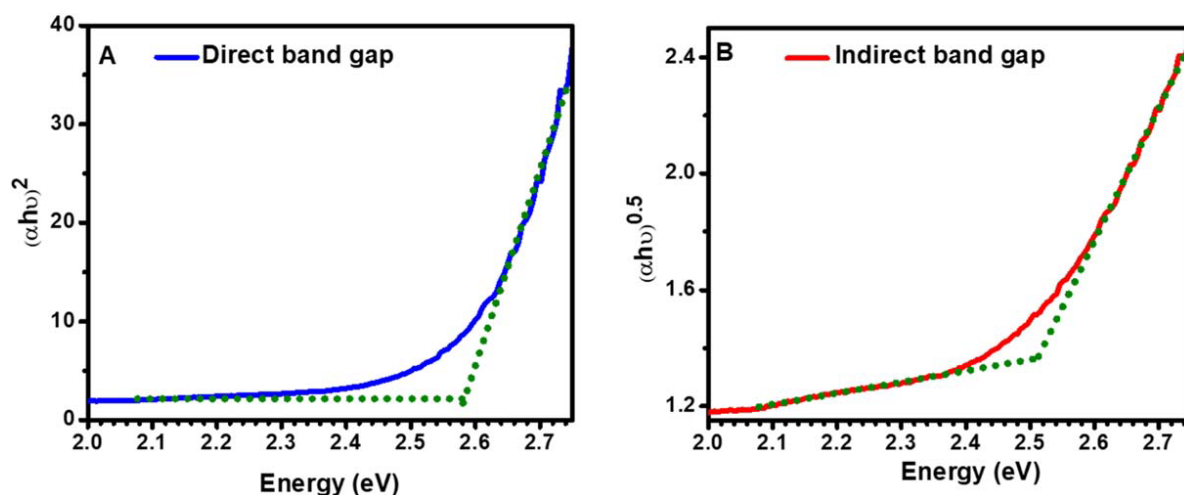
Surface photovoltage spectroscopy (SPS) was deployed to measure the (surface) band gap of as-prepared $\text{Ag}_4\text{V}_2\text{O}_7$. Figure S9B contains the data; from the intercept of this spectrum, the band gap was estimated as: $2.10 \pm 0.03\text{ eV}$. Note that the measured photovoltage onset wavelength ($\sim 600\text{ nm}$) is higher than the measured absorbance onset wavelength ($\sim 530\text{ nm}$, Table I) by the DRS method. This difference possibly originates from the variant sensitivity of SPS and DRS to the surface properties. Specifically, SPS is more sensitive to the sub-band gap energy levels on the semiconductor surface than DRS.³⁶ Also, increasing photovoltage values (Fig. S9A), show that the prepared silver pyrovanadate is a *p*-type semiconductor.

The Fermi level (E_F) of $\text{Ag}_4\text{V}_2\text{O}_7$ was measured by using Kelvin-probe spectroscopy. Figure S10 contains the resultant contact potential difference data; from these, the measured E_F value translates to $-4.84 \pm 0.02\text{ eV}$ on the vacuum energy scale. Using the obtained VBM, E_F , and the surface band gap values, the surface band structure of $\text{Ag}_4\text{V}_2\text{O}_7$ was constructed (Fig. 8). The purple dashed line in the diagram shows the Fermi level located 0.07 eV above the valence band, as expected for a moderately doped *p*-type semiconductors. The valence band position is not favorable for water photooxidation since it lies above the thermodynamic threshold value of $+1.23\text{ V}$ (vs NHE). On the other hand, the conduction band minimum (CBM) is thermodynamically favorable for hydrogen evolution (HER) and oxygen reduction reactions. Significantly, the CBM lies at considerable overpotentials above the HER threshold of 0 V (vs NHE).

Electrochemical and photoelectrochemical (PEC) behavior.—To probe the electrochemical stability of $\text{Ag}_4\text{V}_2\text{O}_7$ in the dark, cyclic voltammetry experiments were performed in aqueous and non-aqueous solutions; Fig. 9A contains the data. In aqueous 0.2 M sodium sulfate, the as-prepared $\text{Ag}_4\text{V}_2\text{O}_7$ electrode showed significant cathodic current on scanning negatively from the open circuit potential. The onset of this cathodic current was $\sim +0.32\text{ V}$; an anodic wave was seen on the return scan. The faint reduction wave and corresponding oxidation wave on the return scan in the non-aqueous case can be attributed to residual traces of water in acetonitrile. The same features were observed previously for AgVO_3 and Ag_3VO_4 ^{23,24} and confirmed that anodic wave seen on the return scan could be attributed to oxidative stripping of metallic silver and generation of Ag^+ species. Therefore, the cathodic corrosion of $\text{Ag}_4\text{V}_2\text{O}_7$ in the presence of water is given as follows:

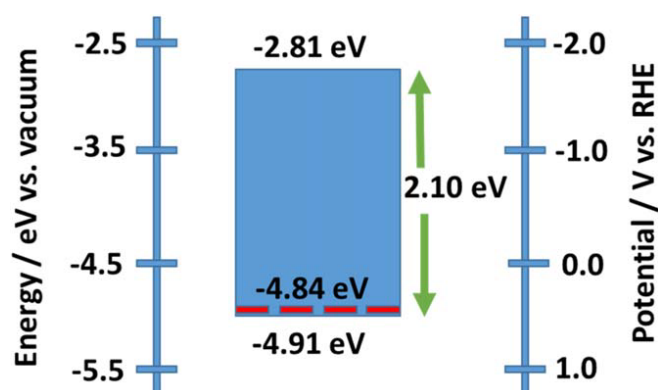
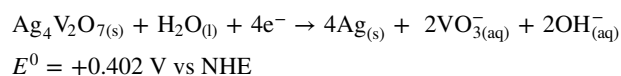
Table I. Absorption onset wavelength value for $\text{Ag}_4\text{V}_2\text{O}_7$ along with literature data.

| | | | | | | | | |
|----------------------------------|------------|-----|-----|-----|-----|-----|-----|-----|
| Absorption onset wavelength (nm) | 530 | 512 | 525 | 563 | 515 | 517 | 496 | 496 |
| References | This study | 4 | 5 | 7 | 10 | 13 | 14 | 31 |

**Figure 7.** Tauc plots for $\text{Ag}_4\text{V}_2\text{O}_7$ film on FTO. Frames (a) and (b) contain the plots analyzed for direct and indirect optical transitions respectively.**Table II.** Energy bandgap values for $\text{Ag}_4\text{V}_2\text{O}_7$ (cf., Fig. 6) along with literature data.

| | | | | | | | |
|------------------------|-----------------|------|------|------|------|------|------|
| Direct band gap (eV) | 2.58 ± 0.04 | 2.71 | 2.47 | 2.50 | 2.45 | NR | 2.25 |
| Indirect band gap (eV) | 2.52 ± 0.02 | NR | NR | NR | NR | 2.31 | NR |
| References | This study | 4 | 5 | 6 | 8 | 15 | 32 |

NR: Not reported

**Figure 8.** Surface energy band positions for as-prepared $\text{Ag}_4\text{V}_2\text{O}_7$ constructed from AP-UPS, Kelvin probe microscopy, and SPS data. Purple dashed line shows the Fermi level position.

[5]

The standard potential for the above reaction was calculated from thermodynamic data culled from the literature on standard Gibbs free energies of formation.^{28,37} These calculations and the underlying data, are summarized in the Supporting Information.

Given the reasonable electrochemical stability of $\text{Ag}_4\text{V}_2\text{O}_7$ in a non-aqueous electrolyte (Fig. 9A), photoelectrochemical (PEC) experiments were conducted using dioxygen as an electron acceptor in a non-aqueous electrolyte. Figure 9B contains the corresponding photovoltage vs time plot for as-prepared $\text{Ag}_4\text{V}_2\text{O}_7$. The positive photovoltage during illumination is in line with the *p*-type semiconductor behavior of $\text{Ag}_4\text{V}_2\text{O}_7$ (see above). The arc-shape of the photovoltage transients is diagnostic of sluggish charge transfer kinetics at the $\text{Ag}_4\text{V}_2\text{O}_7$ /redox electrolyte interface. Linear sweep photovoltammetry (LSV) in dioxygen-purged 0.2 M tetrabutylammonium perchlorate in acetonitrile (Fig. 10A), confirmed the *p*-type semiconductor behavior for electrodeposited $\text{Ag}_4\text{V}_2\text{O}_7$ thin film as it showed cathodic photocurrent polarity under negative (reverse) applied bias potentials. Thus, the photocurrents are generated by minority carriers which are electrons for a *p*-type $\text{Ag}_4\text{V}_2\text{O}_7$ thin film.

Unfortunately, there was significant dark-current flow on applying negative overpotentials during the photovoltammetry experiment, Fig. 10A. To confirm the origin of the increased background cathodic current due to light, both samples after reduction in dark and chopped-light illumination were anodically stripped in acetonitrile contained 0.2 M tetrabutylammonium perchlorate. The results are shown in Fig. 10B. The higher anodic current for the illuminated sample compared to the non-illuminated sample confirmed the acceleration of cathodic corrosion due to irradiation.

Conclusions

In summary, a hybrid cathodic/anodic electrosynthesis technique was developed for preparing $\text{Ag}_4\text{V}_2\text{O}_7$ thin films on FTO substrates. These films were characterized by a range of techniques to furnish information on the morphological, structural, optical, and electronic

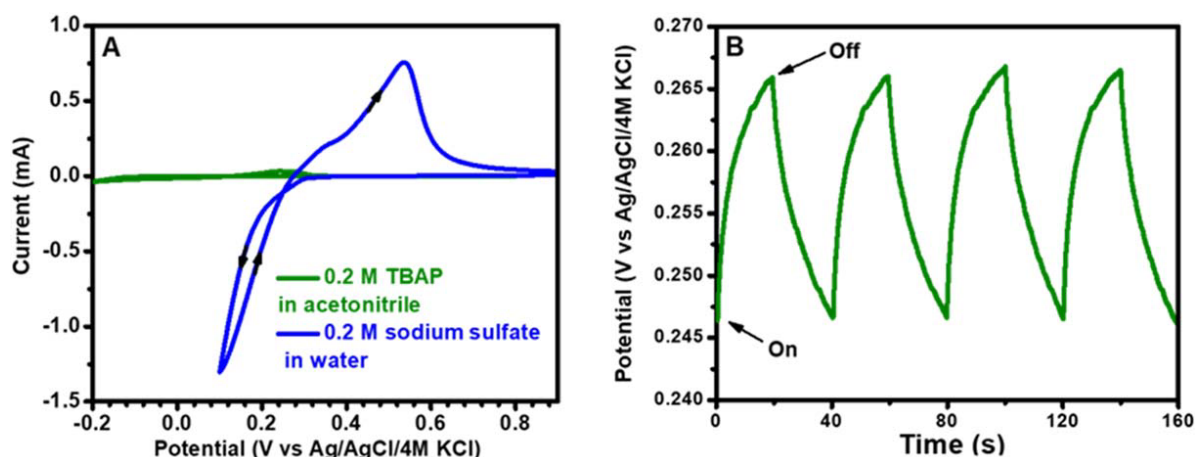


Figure 9. (A) Cyclic voltammograms of as-prepared $\text{Ag}_4\text{V}_2\text{O}_7$ film in 0.2 M sodium sulfate in water and 0.2 M tetrabutylammonium perchlorate in acetonitrile, 25 mV s^{-1} potential scan rate. (B) Photovoltage transients for $\text{Ag}_4\text{V}_2\text{O}_7$ in dioxxygen-purged 0.2 M tetrabutylammonium perchlorate in acetonitrile.

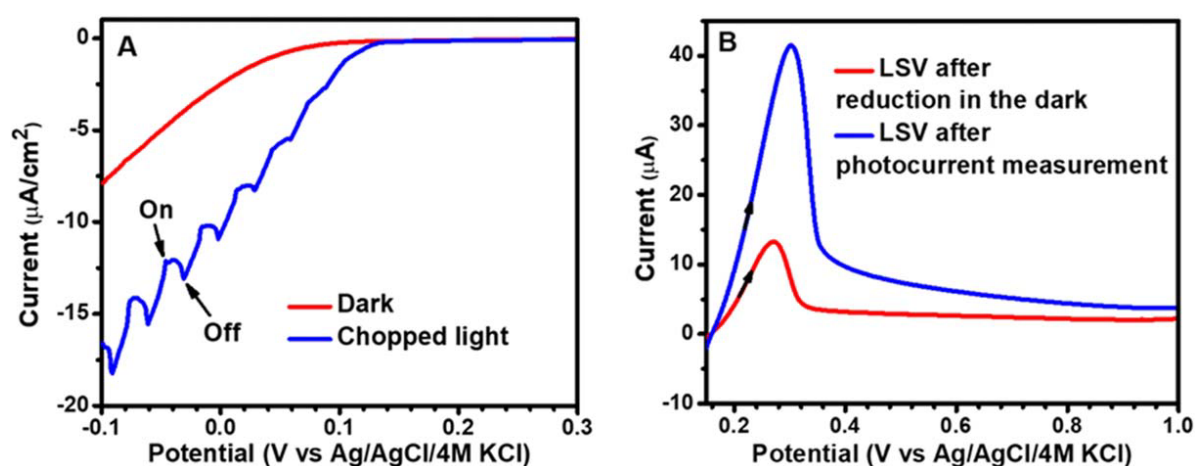


Figure 10. (A) LSV in dark and under chopped-light illumination for $\text{Ag}_4\text{V}_2\text{O}_7$ in dioxxygen-purged 0.2 M tetrabutylammonium perchlorate in acetonitrile, 1 mV s^{-1} potential scan rate. (B) LSV after reduction experiments in dark and under chopped illumination (voltammogram and photovoltammogram in Fig. 9A), in 0.2 M tetrabutylammonium perchlorate in acetonitrile, 10 mV s^{-1} potential scan rate.

band structure of the electrosynthesized *p*-type semiconductor. The applicability of these films in solar energy conversion and environmental remediation schemes as well as other, yet unforeseen practical technologies, would require further research.

Acknowledgments

This work was primarily supported by the National Science Foundation UTA/NU Partnership for Research and Education in Materials (NSF DMR-2122128). P.S.T and C. J. acknowledge funding under the European Union's Horizon Europe Research and Innovation Program from the European Research Council (ERC, Grant Agreement No. 101043617). N. M. thanks the Basic Science Research Program through the National Research Foundation of Korea (NRF), Ministry of Education (Grant NRF-2016R1D1A1B02010133). Finally, the two anonymous reviewers are thanked for their constructive criticisms of an earlier manuscript version.

ORCID

Krishnan Rajeshwar  <https://orcid.org/0000-0003-4917-7790>

References

- M. T. Galante, P. Sotelo, M. K. Hossain, A. Vali, A. Raamann, C. Longo, R. T. Macaluso, and K. Rajeshwar, "Silver oxide-based semiconductors for solar fuels production and environmental remediation: a solid-state chemistry approach." *Chem. Electro. Chem.*, **6**, 87 (2019).
- K. Rajeshwar and A. Vali, *ECS Meet. Abstr.*, **MA2021-02**, 645 (2021).
- S. Kittaka, S. Nishida, and T. Ohtani, "Mechanochemical reactions between Ag_2O and V_2O_5 to form crystalline silver vanadates." *J. Solid State Chem.*, **169**, 139 (2002).
- X. Y. Yuan, F. R. Wang, J. K. Liu, and X. H. Yang, "Thermal perturbation nucleation and controllable growth of silver vanadate crystals by dynamic template route." *Cryst. Growth Des.*, **17**, 4254 (2017).
- N. D. Van and N. T. H. Le, "{0 0 1}-Facet-exposed $\text{Ag}_4\text{V}_2\text{O}_7$ nanoplates: additive-free hydrothermal synthesis and enhanced photocatalytic activity." *J. Nanomater.*, **8462764**, 1 (2018).
- J. Wang, X. Yang, J. Chen, J. Xian, S. Meng, Y. Zheng, Y. Shao, and D. Li, "Photocatalytic activity of novel $\text{Ag}_4\text{V}_2\text{O}_7$ photocatalyst under visible light irradiation." *J. Am. Ceram. Soc.*, **97**, 267 (2014).
- C.-M. Huang, G.-T. Pan, Y.-C. M. Li, M.-H. Li, and T. C.-K. Yang, "Crystalline phases and photocatalytic activities of hydrothermal synthesis Ag_3VO_4 and $\text{Ag}_4\text{V}_2\text{O}_7$ under visible light irradiation." *Appl. Catal. A*, **358**, 164 (2009).
- R. C. de Oliveira, L. Gracia, M. Assis, M. Siu Li, J. Andres, E. Longo, and L. S. Cavalcante, "Disclosing the electronic structure and optical properties of $\text{Ag}_4\text{V}_2\text{O}_7$ crystals: experimental and theoretical insights." *CrystEngComm*, **18**, 6483 (2016).
- T. A. Albrecht, C. L. Stern, and K. R. Poeppelmeier, "The $\text{Ag}_2\text{O-V}_2\text{O}_5\text{-HF(aq)}$ system and crystal structure of $\alpha\text{-Ag}_3\text{VO}_4$." *Inorg. Chem.*, **46**, 1704 (2007).
- C. C. Chena, J. Shayab, H. J. Fanc, Y. K. Changd, H. T. Chia, and C. S. Lu, "Silver vanadium oxide materials: controlled synthesis by hydrothermal method and efficient photocatalytic degradation of atrazine and CV dye." *Sep. Purif. Technol.*, **206**, 226 (2018).
- C. M. Huang, G. T. Pan, L. C. Chen, T. C. K. Yang, and W. S. Chang, "Effects of synthesis conditions on the crystalline phases and photocatalytic activities of silver vanadates via hydrothermal method." *MRS Online Proceedings Library.*, **1171**, 17 (2009).
- R. Masse, M. T. Averbuch-Pouchot, A. Durif, and J. C. Guitel, "Chemical preparation and crystal structure of silver pyrovanadate, $\text{Ag}_4\text{V}_2\text{O}_7$." *Acta Cryst.*, **39**, 1608 (1983).

13. R. Kanta, H. Kato, H. Kobayashi, and A. Kudo, "Photophysical properties and photocatalytic activities under visible light irradiation of silver vanadates." *Phys. Chem. Chem. Phys.*, **5**, 3061 (2003).
14. J. Wang, J. Chen, Y. Yu, W. Yu, X. Meng, J. Chen, and D. Li, "SDS-assisted hydrothermal one-step synthesis and photoelectrochemical study of $\text{Ag}_4\text{V}_2\text{O}_7$ nanorods decorated with Ag nanoparticles." *CrystEngComm*, **17**, 6661 (2015).
15. M. Assis et al., "Bactericidal activity of $\text{Ag}_4\text{V}_2\text{O}_7/\beta\text{-AgVO}_3$ heterostructures against antibiotic-resistant." *Klebsiella Pneumoniae. Biomater. Adv.*, **141**, 213097 (2022).
16. C. Ren, J. Fan, S. Liu, W. Li, F. Wang, H. Li, X. Liu, and Z. Chang, "One-step hydrothermal synthesis of novel $\text{Ag}_3\text{VO}_4/\text{Ag}_4\text{V}_2\text{O}_7$ composites for enhancing visible-light photocatalytic performance." *RSC Adv.*, **6**, 95156 (2016).
17. K. Rajeshwar, "Electrosynthesized thin films of group II–VI compound semiconductors, alloys and superstructures." *Adv. Mater.*, **4**, 23 (1992).
18. T. E. Schlesinger, K. Rajeshwar, and N. R. de Tacconi, "Electrodeposition of semiconductors." *Modern Electroplating*, ed. M. Schlesinger and M. Paunovic (Berlin)(Springer) Chap. 14, p. 383 (2010).
19. K. Rajeshwar, N. R. de Tacconi, and C. R. Chenthamarakshan, "Semiconductor-based composites: preparation, properties, and performance." *Chem. Mater.*, **13**, 2765 (2001).
20. C. Janáky and K. Rajeshwar, "The role of (photo)electrochemistry in the rational design of hybrid conducting polymer/semiconductor assemblies: from fundamental concepts to practical applications." *Prog. Poly. Sci.*, **43**, 96 (2015).
21. C. Janáky, E. Kescenovity, and K. Rajeshwar, "Electrodeposition of inorganic oxide/nanocarbon composites: opportunities and challenges." *Chem. Electro. Chem.*, **3**, 181 (2016).
22. D. Kang, T. W. Kim, S. R. Kubota, A. C. Cardiel, H. G. Cha, and K.-S. Choi, "Electrochemical synthesis of photoelectrodes and catalysts for use in solar water splitting." *Chem. Rev.*, **115**, 12839 (2015).
23. A. Vali, H. P. Sarker, H.-W. Jee, A. Kormányos, F. Firouzan, N. Myung, K.-J. Paeng, M. N. Huda, C. Janáky, and K. Rajeshwar, "Electrodeposition of silver vanadate films: a tale of two polymorphs." *Chem. Phys. Chem.*, **20**, 2635 (2019).
24. A. Vali, P. S. Toth, H.-W. Jee, F. Firouzan, C. Janáky, K.-J. Paeng, N. Myung, and K. Rajeshwar, "Electrosynthesis and properties of crystalline and phase-pure silver orthovanadate." *J. Phys. Chem. C*, **124**, 1980 (2020).
25. A. Vali, H.-W. Jee, N. Myung, and K. Rajeshwar, "Combining electrosynthesis with thermolysis: a safe/scalable route to multinary oxide semiconductor films." *ChemElectroChem*, **8**, 1251 (2021).
26. N. Myung, S. Ham, S. Choi, Y. Chae, W.-G. Kim, Y. J. Jeon, K.-J. Paeng, W. Chanmanee, N. R. de Tacconi, and K. Rajeshwar, "Tailoring interfaces for electrochemical synthesis of semiconductor films: BiVO_4 , Bi_2O_3 , or composites." *J. Phys. Chem. C*, **115**, 7793 (2011).
27. H. T. S. Britton and R. A. Robinson, "Physicochemical studies of complex acids. part IV. the vanadates of silver." *J. Chem. Soc.*, 2328 (1930).
28. C. F. Baes and R. E. Messmer, *The Hydrolysis of Cations* (New York)(Wiley) Chap. 10, p. 197 (1976).
29. M. R. Deakin and D. A. Buttry, "Electrochemical applications of the quartz crystal microbalance." *Anal. Chem.*, **61**, 1147A (1989).
30. D. A. Buttry, "Applications of the quartz crystal microbalance to electrochemistry." *In Electroanalytical Chemistry: A Series of Advances*, ed. A. J. Bard (New York, Marcel Dekker) Vol. 17 (1991).
31. R. Rana, J. G. McEvoya, and Z. Zhang, " $\text{Ag}_2\text{O}/\text{Ag}_3\text{VO}_4/\text{Ag}_4\text{V}_2\text{O}_7$ heterogeneous photocatalyst prepared by a facile hydrothermal synthesis with enhanced photocatalytic performance under visible light irradiation." *Mater. Res. Bull.*, **74**, 140 (2016).
32. D. Zhou, Y. Y. Wang, F. R. Wang, J. K. Liu, and X. M. Zhang, "Design and application of $\text{Ag}_3\text{PO}_4/\text{Ag}_4\text{V}_2\text{O}_7$ Z-scheme photocatalysts with a micro-nano tube-cluster structure for the Co-degradation of nitrate and ammonia in wastewater." *Ind. Eng. Chem. Res.*, **58**, 18027 (2019).
33. A. B. Murphy, "Band-gap determination from diffuse reflectance measurements of semiconductor films, and application to photoelectrochemical water-splitting." *Sol. Energy Mater. Sol. Cells*, **91**, 1326 (2007).
34. D. Roy, G. Samu, M. Hossain, C. Janáky, and K. Rajeshwar, "On the measured optical bandgap values of inorganic oxide semiconductors for solar fuels generation." *Catal. Today*, **300**, 136 (2018).
35. B. D. Vezibic, S. Patel, B. E. Davis, and D. P. Birnie, "Evaluation of the tauc method for optical absorption edge determination: ZnO thin films as a model system." *Phys. Status Solidi B*, **252**, 1700 (2015).
36. I. D. Baikie, A. C. Grain, J. Sutherland, and J. Law, "Ambient pressure photoemission spectroscopy of metal surfaces." *Appl. Surf. Sci.*, **323**, 45 (2014).
37. G. V. Zhutavaeva, N. A. Shumilova, and Y. Israel, "Silver and Vanadium." *Standard Potentials in Aqueous Solution*, ed. A. J. Bard et al. (New York, Marcel Dekker) Chap. 11, p. 295 (1985).